CrystEngComm

Accepted Manuscript

ROYAL SOCIETY OF CHEMISTRY

www.rsc.org/crystengcomm

Journal Name

RSCPublishing

ARTICLE

Cite this: DOI: 10.1039/x0xx00000x

An alternative strategy to construct Fe(II)-based MOFs with multifarious structures and magnetic behaviors

Received 00th January 2012,
Accepted 00th January 2012

DOI: 10.1039/x0xx00000x

www.rsc.org/

Qipeng Li,[a,b] Chongbin Tian,[a] Huabin Zhang,[a] Jinjie Qian,[a,b] and Shaowu Du*[a]

An alternative strategy using cyclopentadienyliron dicarbonyl dimer as starting material has been applied to construct six new Fe(II)-based MOFs, formulated as $[Fe_2(Nic)_4(\mu\text{-}H_2O)]\cdot CH_3CN$ (**1**), $[Fe(PIP)(H_2O)]\cdot H_2O$ (**2**), $[Fe(Hbidc)(H_2O)]$ (**3**), $[Fe(Hbidc)]$ (**4**), $[Fe(Py\text{-}3,4\text{-}BDC)(H_2O)_2]\cdot H_2O$ (**5**) and $[Fe(Py\text{-}3,4\text{-}BDC)(H_2O)_2]$ (**6**) (HNic = nicotinic acid, H_2PIP = 5-(pyridin-4-yl) isophthalic acid, H_3bidc = benzimidazole-5,6-dicarboxylic acid and Py-3,4-H_2BDC = 3,4-pyridinedicarboxylic acid). X-ray Structural analysis reveals that **1** possesses a 3D framework while the rest of compounds are 2D layer structures which are further connected by hydrogen bonding into 3D supramolecular architectures. Magnetic analyses have been performed with the classical spin approximation, revealing that **2**, **5** and **6** exhibit ferromagnetic interactions between Fe(II) ions, while **3** and **4** show antiferromagnetic interactions between Fe(II) centres. The successful preparation of compounds **1**–**6** may provide an alternative and useful approach for the synthesis of Fe(II)-based MOFs in the future.

Introduction

Metal-organic frameworks (MOFs) have attracted great interest not only due to their intriguing topologies and fascinating structures but also because of their potential applications as functional materials in the fields of gas separation, storage, and magnetism.[1] Over the past few decades, much effort has been devoted for developing magnetic MOFs with the concepts of molecular magnetism by modifying metal ions or constructing various structures with different organic ligands.[2] In consideration of the nature of metals that greatly influences the magnetic behaviours, the 3d transition metals could be the best candidates to introduce significant magnetic properties in the molecular magnetic materials.[3] To date, a large number of such materials with 3d transition metals (e.g. Mn, Co, Ni and Cu) have synthesized and their magnetic properties have been extensively studied.[4] By comparison, those with iron metal are relatively rare because iron MOFs are more difficult to prepare possibly due to the fact that Fe(II) is readily oxidized to Fe(III), which is subsequently hydrolyzed under hydrothermal conditions, resulting in the formation of ferric oxide.[5] One way to prevent the hydrolysis of ferric ion is to employ hydrofluoric acid as a mineralizing agent to eliminate the influence of the hydroxide ions, for example, in the synthesis of well-known families of MIL-53, MIL-62 and MIL-68.[6] Another way to avoid the hydrolysis is to use non-aqueous solvents such as DMF (*N*,*N*′-Dimethylformamide) or mixed solvent of pyridine and ethanol, as demonstrated by the synthesis of MOF-235 and MOF-236.[7] Despite some success, there remains the necessity to develop more effective and convenient synthetic methods for the iron magnetic MOF materials.

N-containing aromatic carboxylic acids, which have mixed *N*,*O*-donor systems are a family of good ligands in coordination chemistry due to their strong coordination ability and versatile coordination modes, and have been widely used in the assembly of MOFs, in particular with 3d metals. For example, a large number of Mn, Co, Cu and Ni-based MOFs with HNic, H_2PIP, H_3bidc and Py-3,4-H_2BDC ligands have been synthesized (HNic = nicotinic acid, H_2PIP = 5-(pyridin-4-yl) isophthalic acid, H_3bidc = benzimidazole-5,6-dicarboxylic acid and Py-3,4-H_2BDC = 3,4-pyridinedicarboxylic acid).[8] However, so far only five examples of Fe(II)-based MOFs, one with Py-3,4-H_2BDC and the others with HNic ligands have been reported.[9] In the present work, we have developed an alternative strategy for the synthesis of iron MOFs by utilizing $[Fe(Cp)(CO)_2]_2$ (Cp = cyclopentadiene) instead of other common iron salts, which leads to the successful isolation of six new Fe(II)-based MOFs, namely $[Fe_2(Nic)_4(\mu\text{-}H_2O)]\cdot CH_3CN$ (**1**), $[Fe(PIP)(H_2O)]\cdot H_2O$ (**2**), $[Fe(Hbidc)(H_2O)]$ (**3**), $[Fe(Hbidc)]$ (**4**), $[Fe(Py\text{-}3,4\text{-}BDC)(H_2O)_2]\cdot H_2O$ (**5**) and $[Fe(Py\text{-}3,4\text{-}BDC)(H_2O)_2]$ (**6**). Herein, their syntheses, crystal structures and magnetic properties are discussed in detail.

Experimental

Materials and methods

All the starting materials and solvents were commercially available and used as purchased without further purification. Thermo-gravimetric experiments were performed using a TGA /NETZSCH STA-449C instrument heated from 30–1000ºC (heating rate of 10ºC/min, nitrogen stream). IR spectra were recorded on a Spectrum-One FT-IR spectrophotometer using KBr pellets. Powder X-ray diffraction (PXRD) patterns were recorded on a PAN alytical X'pert PRO X-ray Diffractometer with crushed single crystals in the 2θ range 5–55° using Mo-Kα radiation. Element analyses for C, H and N were measured with an Elemental Vairo ELIII analyzer. Polycrystalline magnetic susceptibility data were collected on Quantum Design MPMS (SQUID)-XL magnetometer and PPMS-9T system.

Synthesis of $[Fe_2(Nic)_4(\mu\text{-}H_2O)]\cdot CH_3CN$ (1). A mixture of HNic (62.0 mg, 0.50 mmol) and $[Fe(Cp)(CO)_2]_2$ (46.8 mg, 0.125 mmol) were placed in a 20 ml of Teflon-lined stainless steel vessel with 7.0 ml of CH_3CN/H_2O (v/v: 4:3). The mixtures were heated to 160 ºC in 4 h and kept at this temperature for two days and subsequently cooled slowly to room temperature during another two days. Yellow crystals of **1** were obtained.

Synthesis of $[Fe(PIP)(H_2O)]\cdot H_2O$ (2). The procedure was analogous to that for **1**, except that H_2PIP was used instead of HNic. Yellow crystals of **2** were obtained in 50% yield based on $[Fe(Cp)(CO)_2]_2$. Elemental Anal. Calcd. for $C_{13}H_{11}FeNO_6$ (%): C 46.88, H 3.33, N 4.21. Found (%): C 47.23, H 3.09, N 4.17. IR (KBr pellets, cm^{-1}): 3568s, 1610.12m, 1514s, 1462m, 1341w, 838m, 775m, 719w, 649m.

Synthesis of $[Fe(Hbidc)(H_2O)]$ (3) and $[Fe(Hbidc)]$ (4). A mixture of H_3bidc (103 mg, 0.50 mmol) and $[Fe(Cp)(CO)_2]_2$ (46.8 mg, 0.125 mmol) was placed in a 20 ml of Teflon-lined stainless steel vessel with 7.0 ml of CH_3CN/H_2O (v/v: 4:3). The mixture was heated from room temperature to 160 ºC in 4 h, and kept at this temperature for two days. The reaction system was cooled slowly to room temperature during another two days. Compound **3** was prepared similarly except that toluene was used instead of CH_3CN. Yellow crystals of **3** and **4** were separated manually with 50 and 72% yields, respectively based on $[Fe(Cp)(CO)_2]_2$. Elemental Anal. Calcd. for **3** $C_9H_6FeN_2O_5$ (%): C, 38.85; H, 2.18; N, 10.08. Found (%): C, 39.02; H, 2.34; N, 10.32. For **4**: $C_9H_4FeN_2O_4$ (%): C, 41.55; H, 1.55; N, 10.77. Found (%): C, 41.20; H, 1.52; N, 10.36. IR (KBr, cm^{-1}) for **3**: 3399s, 1866vw, 1637s, 1547m, 1508w, 1481m, 1440m, 1411m, 1347m, 1257m, 1123m, 966w, 884w, 802w, 675m, 597vw, 541 w, 495w. For **4**: 3119w, 2929m, 1863w, 1603m, 1525s, 1477s, 1412w, 965m, 806m, 636m.

Synthesis of $[Fe(Py\text{-}3,4\text{-}BDC)(H_2O)_2]\cdot H_2O$ (5) and $[Fe(Py\text{-}3,4\text{-}BDC)(H_2O)_2]$ (6). The procedure was analogous to **3**, except that Py-3,4-H_2BDC was used instead of H_3bidc. Orange crystals of **5** and yellow crystals of **6** were obtained in 32 and 45% yields respectively based on $[Fe(Cp)(CO)_2]_2$. Elemental anal. calcd. for **5**: $C_7H_9FeNO_7$ (274.99): C, 30.55; H, 3.30; N, 5.09%. Found: C, 30.30; H, 3.18; N, 5.23%. For **6**: $C_7H_7FeNO_6$ (256.99): C, 32.72; H, 2.75; N, 5.45%. Found: C, 32.54; H, 2.95; N, 5.62%. IR (KBr, cm^{-1}) for **5**: 3841 w, 3737 w, 2360 w, 1557 vw, 1406 vw, 1229 w, 1173 w, 840 m, 779 s, 712 m, 681w. For **6**: 3467 s, 1968 vw, 1621 s, 1555 w, 1538 w, 1401 m, 1296 w, 1223vw, 1066m, 872m, 841 vw, 715 m, 606 m.

X-ray Structure Determination

Single-crystal X-ray diffraction data were collected on a Rigaku diffractometer with a Mercury CCD area detector (Mo Kα; λ = 0.71073 Å). Empirical absorption corrections were applied to the data using the Crystal Clear program.[10] The structures were solved by direct method and refined by full-matrix least-squares on F^2 using the SHELXTL-97 program.[11] Metal atoms in each complex were located from the E-maps and other non-hydrogen atoms were located in successive difference Fourier syntheses. All non-hydrogen atoms were refined anisotropically. The organic hydrogen atoms were positioned geometrically, while those of the water molecules were located using the difference Fourier method. Crystallographic data and other pertinent information for **1**–**6** are summarized in Table 1. Selected bond lengths and angles are listed in Table S1–S6. Bond lengths and angles of hydrogen bonds are listed in Table S7–S11. The CCDC numbers for **1**–**6** are 930763 and 930765–930769, respectively.

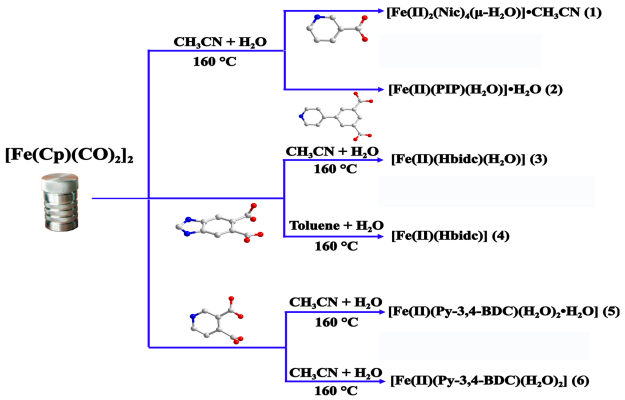

Scheme 1 The syntheses of six Fe(II)-based MOFs.

Results and discussion

Synthesis

Hydro(solvo)thermal synthesis is a convenient and powerful synthetic technique for the preparation of metal-carboxylate frameworks, which involves the self-assembly of metal ions with carboxylate ligands. In comparison with other transition metals, the number of iron-carboxylate MOFs is rather limited because of the facile hydrolysis of ferric ions in solution[5]. In our studies, we find that the use of $[Fe(Cp)(CO)_2]_2$ instead of other common iron salts in the preparation of iron MOFs under hydro(solvo)thermal conditions can help in preventing the hydrolysis of ferric ions, thought the underlying cause is not clear due to the complexity involved in hydro(solvo)-thermal reaction at high temperature and pressure conditions. Thus, the

Journal Name RSCPublishing

ARTICLE

Table 1 Pertinent Crystal Data and Structure Refinement Results for Compounds **1**–**6**

Compounds	**1**	**2**	**3**	**4**	**5**	**6**
Formula	$C_{26}H_{21}Fe_2N_5O_9$	$C_{13}H_{11}FeNO_6$	$C_9H_6FeN_2O_5$	$C_9H_4FeN_2O_4$	$C_7H_9FeNO_7$	$C_7H_7FeNO_6$
Mr	659.16	333.08	278.01	259.99	274.99	256.99
Space group	*P*–1	*P*–1	$P2_1/c$	$P2_1/n$	*P*–1	$P2_1/c$
a (Å)	10.48(2)	7.292(3)	9.35(9)	10.18(9)	7.12(3)	10.99(4)
b (Å)	11.84(3)	10.070(4)	6.92(4)	5.96(5)	7.97(3)	10.36(4)
c (Å)	14.03(2)	10.272(4)	14.62(9)	13.31(2)	9.11(4)	7.72(3)
α (deg)	105.65(1)	113.98(3)	90	90	75.89(17)	90
β (deg)	101.22(9)	99.68(1)	104.44 (5)	96.59 (6)	68.64(15)	102.02 (6)
γ (deg)	112.36(5)	103.65(5)	90	90	76.35(16)	90
V (Å^3)	1462.5(5)	639.4(4)	914.7 (2)	802.50 (3)	461.6 (3)	860.5 (6)
Z	2	2	4	4	2	4
D_c (g cm^{-3})	1.05	1.730	2.01	2.15	1.96	1.98
M (mm^{-1})	1.05	1.208	1.66	1.88	1.66	1.76
F(000)	668.0	340	560.0	520.0	276.0	520.0
GOF	1.04	1.040	1.05	0.963	1.07	1.14
R_1[a]	0.035	0.0365	0.033	0.036	0.030	0.038
wR_2[a]	0.127	0.1276	0.124	0.121	0.119	0.098

[a] $R_1 = \sum (||Fo| - |Fc||)/\sum |Fo|$, $wR = \{\sum w[(Fo^2 - Fc^2)^2]/\sum w[(Fo2)^2]\}^{1/2}$

reactions of $[Fe(Cp)(CO)_2]_2$ with four *N*-containing aromatic carboxylic acids afford six new iron-carboxylate MOFs in moderate yields. They cannot be obtained under the same conditions by using other common Fe(II) salts.

On the other hand, in the hydro(solvo)thermal synthesis of MOF materials, except for the type of metal ions and organic ligands, other factors, such as reaction temperature, solvents, pH value of the solution and the counter ions may greatly influence the structures of the final products.[12] As illustrated in Scheme 1, compounds **1** and **2** have been synthesized based on different ligands under the same synthesis conditions, while **3** and **4** are prepared with the same ligand but from different mixed solvents. Compounds **5** and **6** are obtained from the same reaction. Compound **1** is unstable and gradually darkens when exposed to air.

Description of crystal structures

Compound **1** crystallizes in the triclinic space group *P*–1 and its asymmetric unit contains two Fe(II) ions, four Nic^- ligands, one bridging water molecule and one guest CH_3CN molecule. The Fe(II) ions are six-coordinated with a distorted octahedral geometry by two N atoms from two Nic^- ligands, three carboxylate O atoms from another two Nic^- ligands and one water molecule. The Nic^- ligands adopt two types of coordination modes, κ^1-(κ^1-κ^1)-μ_3 and κ^1-κ^1-μ_2 (Scheme S1, A and B) to connect Fe(II) ions into a 3D framework. The Fe1 and Fe2 ions are bridged by two carboxylate groups and one water molecule to form a dinuclear unit (Fig. 1a). The adjacent units are connected by Nic^- ligands to generate a 1D chain (Fig. 1b), which is extended into a 2D layer by pillared Nic^- ligands. These 2D layers are bridged by Nic^- ligands, leading to a 3D framework (Fig. 1c). From the topological point of view, the dinuclear iron unit can be simplified as one node and the ligand as a connector, therefore the whole structure of **1** can be abstracted into a 4-connected *dia* net with the point symbol of {6^6} and the vertex symbol of [6(2).6(2).6(2).6(2).6(2).6(2)][13] (Fig. 1d).

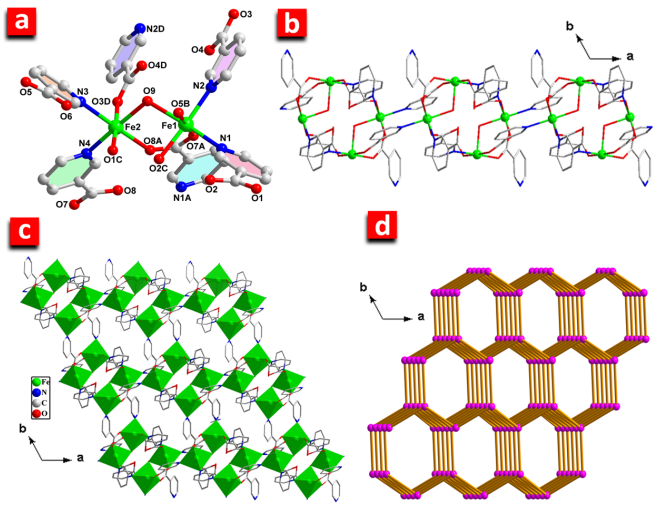

Fig. 1 (a) View of the coordination environment of Fe(II) ions in **1**. Symmetry codes: A $-x-1, -y+1, -z-1$; B $-x-1, -y+2, -z$; C $-x, -y+2, -z$; D $-x-1, -y+2, -z-1$. (b) The 1D chain constructed by the two Fe(II) ions and Nic^- ligands. (c) The 3D structure of **1**. (d) The 3D *dia* structure of **1**.

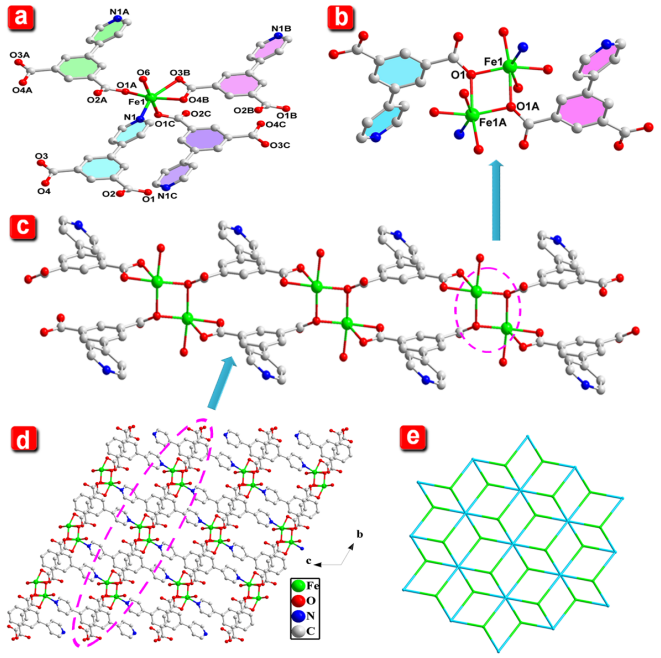

Fig. 2 (a) View of the coordination environment of the Fe(II) ions in **2**. Symmetry codes: A $x-1, y-1, z-1$; B $x-1, y, z-1$; C $-x+2, -y+2, -z+1$; D $x+1, y, z+1$; E $x+1, y+1, z+1$. (b) The diiron unit in **2**. (c). 1D chain constructed by ligand and binuclear iron units. (d) 2D layer framework fabricated by double layer chain structure. (e) The (3,6)-connected 2D framework with a kgd topology network in **2**.

Compound **2** also crystallizes in the triclinic space group *P*–1. The asymmetric unit consists of one Fe(II) ion, one PIP^{2-} ligand, one coordinated and one lattice water molecules. The Fe(II) centre is six-coordinate in a square-bipyramid geometry surrounded by four carboxylate O atoms from three PIP^{2-} ligands, one O atom from the coordinated water molecule and one N atom from another PIP^{2-} ligand (Fig. 2a). All the PIP^{2-} ligands adopt a κ^1-κ^2-μ_2-μ_4 coordination mode (Scheme S1, C) to connect Fe(II) ions into a 2D framework. The Fe1 and its symmetry-related Fe1A ions are bridged by two carboxylate O atoms, forming a dinuclear unit (Fig. 2b). The neighbouring diiron units are linked by two carboxylate groups to generate a 1D chain (Fig. 2c) which is extended by PIP^{2-} ligands into a 2D double-layered structure (Fig. 2d). From the topological point of view, each diiron unit and each PIP^{2-} ligand acts as a 6- and a 3-connected node, respectively. Thus, **2** is a 2D (3,6)-connected *kgd* topological net with the point symbol of {4^3}2{4^6.6^6.8^3} and the vertex symbol of [4.4.4][4.4.4.4.4.6.6.6.6.6.6.*.*.*] (Fig. 2e). In addition, the hydrogen bonds between uncoordinated carboxylates and the O–H groups in coordinated and lattice water molecules extend the 2D layers into a 3D supramolecular architecture (Fig. S1).

Compound **3** crystallizes in the monoclinic space group $P2_1/c$ and its asymmetric unit contains one Fe(II) ion, one $Hbidc^{2-}$ ligand and one coordinated water molecule. The Fe(II) centre adopts a distorted trigonal-bipyramid geometry, and is coordinated by one N atom from a $Hbidc^{2-}$ ligand, three carboxylate O atoms from another three $Hbidc^{2-}$ ligands and one O atom from the coordinated water molecule (Fig. 3a).

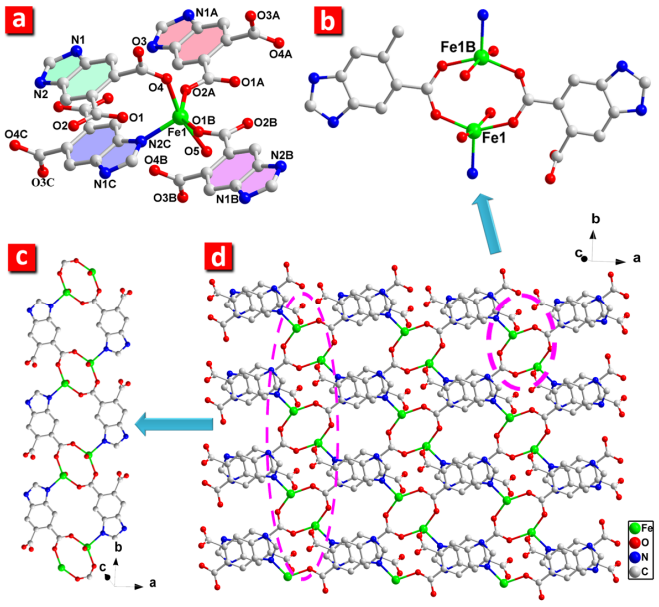

Fig. 3 (a) View of the central Fe(II) coordination environments in **3**. Symmetry codes: A $x, y-1, z$; B $-x+1, -1-y, -z+1$; C $-x, -y, -z+1$; D $x, y+1, z$ (b) The diiron unit in **3**; (c) The 1D chain constructed by ligand and π–π stacking; (d) The 2D framework layer structure of **3**.

The $Hbidc^{2-}$ ligand adopt a κ^1-κ^1-(κ^1-κ^1)-μ_4 coordination mode to connect the Fe(II) ions into a 2D framework (Scheme S1, D). The Fe1 and its neighbouring Fe(II) ions are bridged by two $Hbidc^{2-}$ ligands to give a diiron unit (Fig. 3b), which is linked by $Hbidc^{2-}$ ligands in the *a* and *b* directions to create a typical 2D (3,6)-connected *kgd* topology net (Fig. 3c, 3d and S2). These 2D layers are extended into 3D supramolecular architecture via hydrogen bonds between the uncoordinated carboxylate O atoms and the coordinated water molecule and N–H groups of the imidazole rings (Fig. S3).

Compound **4** crystallizes in the monoclinic space group $P2_1/n$ with the asymmetric unit includes one Fe(II) ion and one $Hbidc^{2-}$ ligand. The Fe(II) centre adopts a distorted trigonal bipyramid geometry, and is coordinated by four carboxylate O atoms from three different $Hbidc^{2-}$ ligands and one imidazole N atom from another $Hbidc^{2-}$ ligand (Fig. 4a). The $Hbidc^{2-}$ ligand adopts a κ^1-(κ^2-κ^2)-μ_4 coordination mode to link Fe(II) ions into a 2D network (Scheme S1, E). In **4**, there exits a $\{FeO\}_n$ left-handed helix and a $\{FeOCO\}_n$ right-handed helix sharing one common axis (Fig. 4b). These helical chains are further linked by the carboxylate groups and imidazole N atoms to generate a 2D layer (Fig. 4c). The hydrogen bonds between uncoordinated carboxylate O atoms and the N–H groups in the imidazole rings extend the 2D layers into a 3D supramolecular framework (Fig. S4).

Compound **5** crystallizes in the triclinic space group *P*–1 and the asymmetric unit contains one Fe(II) ion, one Py-3,4-BDC^{2-} ligand, two coordinate water molecules and one guest water molecule. The Fe(II) centre is six-coordinated by three carboxylate O atoms from three different Py-3,4-BDC^{2-} ligands, one pyridyl N atom from another Py-3,4-BDC^{2-} ligand and two water molecules (Fig. 5a). The completely deprotonated Py-3,4-BDC^{2-} ligands display κ^1-κ^1-(κ^1-κ^1)-μ_4 and κ^1-(κ^1-κ^1-κ^1)-μ_3 coordination modes to connect Fe(II) ions into a 2D structure (Scheme S1, F and G). Two neighbouring

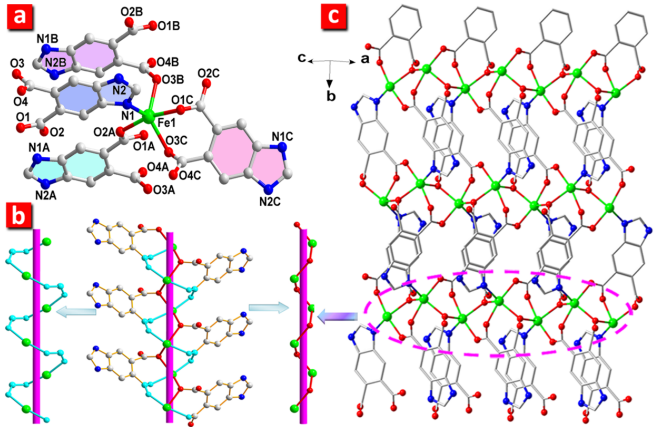

Fig. 4 (a) View of the central Fe(II) coordination environments in **4**. Symmetry codes: A x+1, −y, −z+2; B -x+1, −y+1, −z+2; C x+1/2, −y+1/2, z−1/2; D x−1/2, −y+1/2, z+1/2; (b) View of the double stranded chains; (c) The 2D layer structure of **4**.

Fe(II) ions are linked by the O–C–O bridge of the Py-3,4-BDC^{2-} ligands to form a diiron unit, which is further linked by the pyridine ring to form a 1D chain (Fig. 5b). The adjacent chains are connected by Py-3,4-BDC^{2-} ligand to give a 2D (3,6)-connected *kgd* topological network (Fig. S5). The 2D network of **5** is enlarged into a 3D supramolecular framework through the hydrogen bonding interaction between the O atoms of coordinated water and the uncoordinated carboxyl group (Fig. S6).

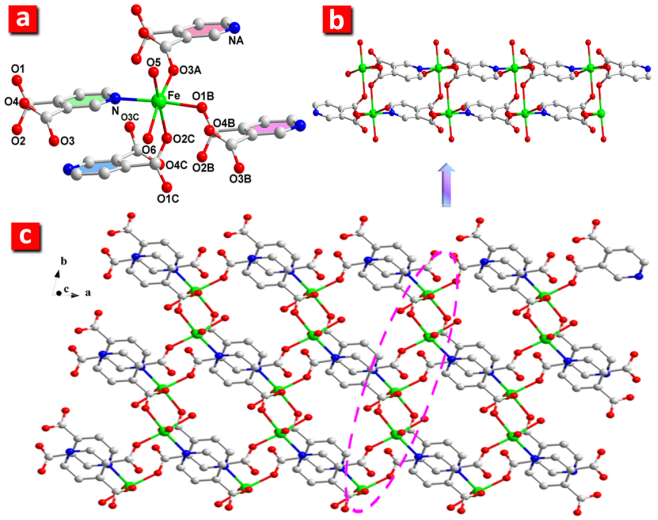

Fig. 5 (a) Representation of the Fe(II) coordination environments of **5**. Hydrogen atoms are omitted for clarity. Symmetry codes: A x−1, y, z; B x−1, y+1, z; C −x+2, −y, −z; D x+1, y−1, z; E x+1, y, z. (b) 1D chain constructed by the ligands and the Fe(II) ions. (c) 2D layer framework of **5**.

Compound **6** crystallizes in the monoclinic space group $P2_1/c$ and the asymmetric unit contains one Fe(II) ion, one Py-3,4-BDC^{2-} ligand and two coordinate water molecules. The Fe(II) centre is six-coordinated by three carboxylate O atoms from two different Py-3,4-BDC^{2-} ligands, one pyridyl N atom from another Py-3,4-BDC^{2-} ligand and two O atoms from coordinated water molecules (Fig. 6a). The completely deprotonated Py-3,4-BDC^{2-} ligand adopts a κ^1-(κ^1-κ^1-κ^1)-μ_3 coordination mode to organize Fe(II) ions into a 2D structure (Scheme S1, G). Each Fe(II) and its neighbouring one are bridged by two Py-3,4-BDC^{2-} ligands to give a diiron unit, which is connected into a 1D chain by the pyridyl N atom (Fig. 6b). The 1D chains are linked by carboxylate groups, resulting in a 2D 4-connected *sql* network (Fig. 6, c and d). The 2D structure of **6** is extended into a 3D supramolecular framework by hydrogen bonds between the pyridyl N atom and the O atom of the coordinated carboxyl group (Fig. S7).

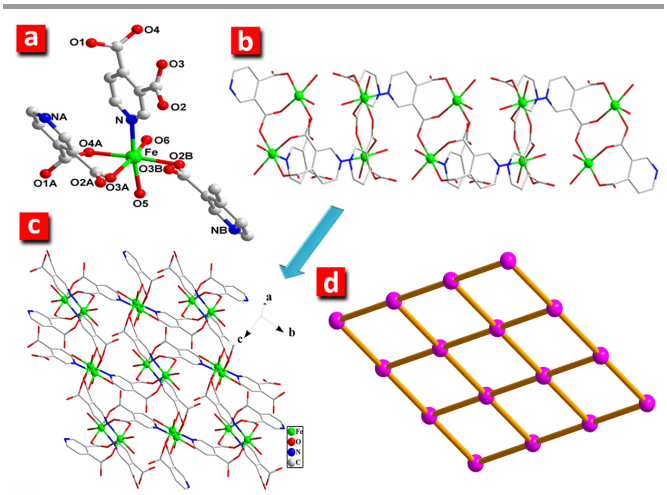

Fig. 6 (a) View of the coordination environment of the central Fe(II) atoms in **6**. Hydrogen atoms are omitted for clarity. Symmetry codes: A x, −y+3/2, z+1/2; B −x+1, y−1/2, −z+3/2; C −x+1, y+1/2, −z+3/2; D x, −y+3/2, z−1/2. (b) View of the 1D chain structure in **6**. (c) View of the 2D layer structure in **6**. (d) The 4-connected 2D framework with a *sql* topology network in **6**.

X-ray diffraction and thermal stability analysis

Powder X-ray diffractions (PXRD) for **1–6** were performed to characterize their purity (Fig. S8). All the diffraction peak positions on the curves are correspond well with their simulated ones, indicating the phase purity of the solids. The TGA curve of **1** indicates that one CH_3CN guest molecule and one coordinated H_2O molecule are lost from 30 to 310°C (obsd. 8.50%, calcd. 8.95%) (Fig. S9) and the framework begins to collapse from 350°C. The TGA curve of **2** exhibits two main steps of weight loss. The first step from 30 to 200°C corresponds to the loss of one lattice water molecule and one coordinated water molecule (obsd. 10.95%, calcd. 10.81%). The second weight loss occurs over the range of 440–540°C is relevant to the gradually decomposition of the framework. The TGA curve of **3** indicates that a coordinated H_2O molecule is gradually released from 30 to 415°C (obsd. 6.18%, calcd. 6.47%) and the framework starts to decompose at about 450°C. There is no weight loss for **4** before decomposition of the framework occurs from 340 to 450°C. Compound **5** shows a weight loss of 19.82% from 40 to 295°C, which is attributed to the loss of two coordinated water molecules and one lattice water molecule (calcd. 19.60%). Then the framework collapses at about 310°C. A weight loss of 14.50% from 40 to 295°C is observed for **6**, which is assigned to the release of two coordinated water molecules (calcd. 14.01%). The decomposition of the framework of **6** occurs at about 320°C.

Magnetic property

The variable-temperature magnetic susceptibility measurement was performed on the polycrystalline samples of **2–6** in the temperature range of 300–2 K, and was shown in Fig. 7–9, respectively, in the form of x_mT–T plots, where x_m is molar magnetic susceptibility per formula unit. It should be noted that the magnetic property of **1** is not reported here due to its poor stability.

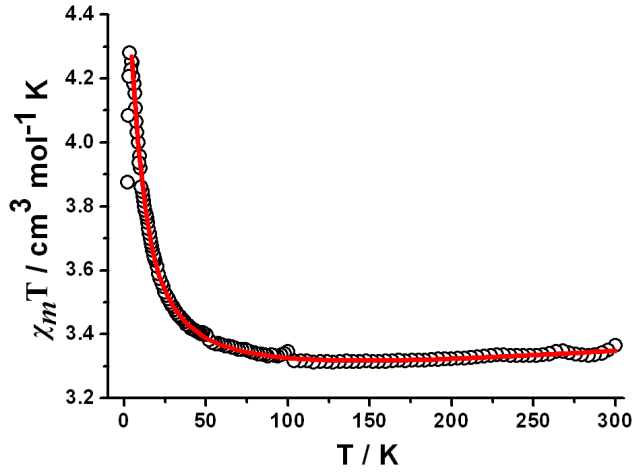

Fig. 7 The plots of x_mT *vs*. T for **2**.

For **2**, at room temperature, the x_mT value is 3.37 emu K mol^{-1}, which is correspond to the g value of 2.12. This is in agreeing with the typical value for a high-spin (HS) Fe(II) with some orbital contributions[14]. As the temperature decreases, the x_mT value increases smoothly until a maximum value of 4.28 cm^3 K mol^{-1} at 3.47 K (Fig.7), and then suddenly drops to 3.88 cm^3 K mol^{-1} at 2 K. This behavior is consistent with the presence of ferromagnetic interaction between Fe(II) centres of the diiron units, while the decreases of the x_mT at low temperature may be caused by the zero-field spitting effect (ZFC). Above 10 K, the magnetic data was fitted by Curie-Weiss equation to give a Curie constant C = 3.32 cm^3 mol^{-1} and Weiss temperature θ = 1.07 K (Fig. S10). The positive value of θ indicates the ferromagnetic interaction. The M vs. H plots (at 2 K) shows that M increases quickly at very low field, and reaching a saturation value of 3.80 Nβ at 8 T, which further confirms the ferromagnetic interactions (Fig. S11).

The x_mT vs. T plots of **3** and **4** exhibit a similar magnetic behaviour (Fig. 8). At 300 K, the x_mT values of **3** and **4** are 3.33 and 3.68 cm^3 K mol^{-1}, respectively, which are close to the expected value for two uncoupled HS Fe(II) ions. Upon cooling, the value of x_mT decreases slightly to a value of 2.78 cm^3 K mol^{-1} for **3** and 3.01 cm^3 K mol^{-1} for **4** at 50 K. Upon further cooling, the sample undergoes a rapid decrease in x_mT reaching 0.60cm^3 K mol^{-1} for **3** and 0.26 cm^3 K mol^{-1} for **4** at 2 K. The magnetic susceptibility data for the plot of x_m vs. T follow Curie-Weiss behaviour in the 10-300 K temperature range (C = 3.67 cm^3 mol^{-1} and θ = –22.23 K for **3** and C = 3.84 cm^3 mol^{-1} and θ = –14.30 K for **4**, Fig. S12 and S14). The negative Weiss constants suggest antiferromagnetic interaction between Fe(II) centres in **3** and **4**. At 2 K and 8 T, the saturated magnetization for **3** and **4** are 2.41 and 1.24 Nβ, respectively, which suggest weak anti-ferromagnetic interactions between the Fe(II) ions (Fig. S13 and S15).

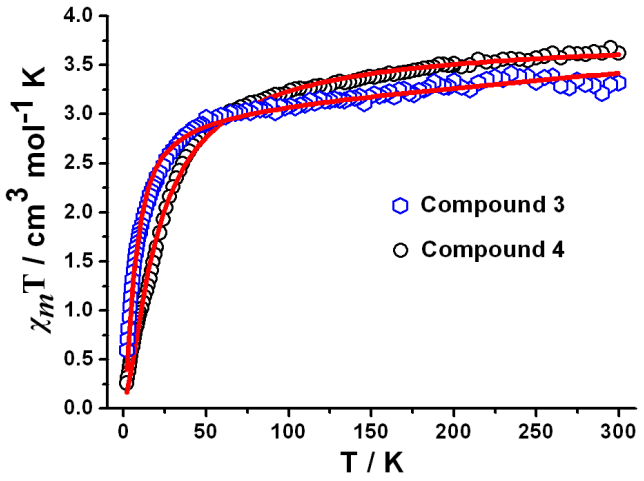

Fig 8 Temperature dependence of x_mT values for **3** and **4**

For **5**, the observed x_mT value at room temperature per Fe(II) ion is 3.30 cm^3 K mol^{-1} (Fig. 9). The x_mT value increases continuously with decreasing temperature, to a maximum value of 3.55 cm^3 K mol^{-1} at 20 K and then decreases abruptly to 2.81 cm^3 K mol^{-1} at 2 K. The x_mT value with a decreasing temperature indicates the presence of ferromagnetic interaction. The sharp decrease of the x_mT value at a very low temperature region may be attributed to zero-field splitting factor and/or interdimer anti-ferromagnetic interactions. The magnetic data above 10 K follow the Curie-Weiss law with a Curie constant of C = 3.20 cm^3 mol^{-1} and a Weiss constant of θ = 1.12 K (Fig. S16). The positive θ value indicates the presence of ferromagnetic interaction between the Fe(II) ions. The ferromagnetic interaction is also supported by the field dependence of the magnetization and the saturated magnetization of 3.68 Nβ at the highest field of 8T (Fig. S17).

Compound **6** exhibits a similar magnetic behavior like **5**. At room temperature, the x_mT value is 3.13 cm^3 K·mol^{-1} (Fig. 9). Upon cooling, the x_mT value increases slightly to a maximum value of 3.45 cm^3 K mol^{-1} at 35.90 K, whereas below 35.90 K, it decreases suddenly and reaches a value of 0.69 cm^3 K mol^{-1} at 2 K. A plot of x_m^{-1} *versus* T for **6** is linear from 10 to 300 K, which follows the Curie-Weiss law with a Curie constant of C = 3.13 cm^3 mol^{-1} and a Weiss constant of θ = 0.96 K (Fig. S18). The positive θ value indicates the presence of ferromagnetic interaction between Fe(II) ions. The ferromagnetic interaction is also sustained by the field dependence of the magnetization and the saturated magnetization at the highest field of 8 T (3.99 Nβ, Fig. S19).

For **2**, **3**, **5** and **6**, the secondary building units (SBUs) of these compounds are two dinuclear Fe(II) units. And thus, to estimate the coupling constants between the Fe(II) ions, a dinuclear mode was adopted. The spin Hamilton of this mode can be written as $H = -JS_1S_2$. The deduced expression of the molar susceptibility x_m is:

$$x_m = 2Ng^2\beta^2/KT((e^{2j/KT} + 5e^{6j/KT} + 14e^{12j/KT} + 30e^{20j/KT})/(1 + 3e^{2j/KT} + 5e^{6j/KT} + 7e^{12j/KT} + 9e^{20j/KT})) + TIP \quad (1)$$

where N, g, β and K have their usual meanings, and J is the exchange constant between adjacent Fe(II) ions, TIP is the

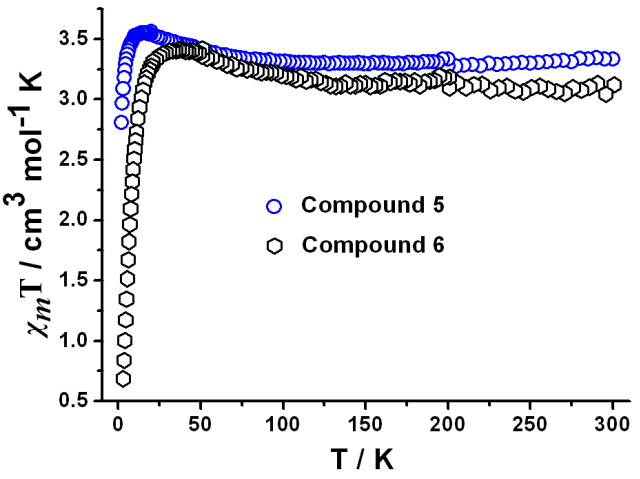

Fig. 9 Temperature dependence of $\chi_m T$ values for **5** and **6**.

temperature-independent paramagnetism. Using equation 1, the best fit for **2** (5−300 K) gives, g = 2.09, J = 0.33 cm^{-1}, $TIP = 6 \times 10^{-5}$ and $R = 9.6 \times 10^{-4}$ (Fig. 7); for **3** (2−300 K): g = 2.03, J = –0.72 cm^{-1}, $TIP = 6.7 \times 10^{-4}$ and $R = 5.4 \times 10^{-4}$ (Fig. 8); for **5** (15−300 K): g = 2.09, J = 0.31 cm^{-1}, $TIP = 3 \times 10^{-5}$ and $R = 5.3 \times 10^{-4}$ (Fig. S20); for **6** (30−300 K): g = 2.01, J = 0.85 cm^{-1}, $TIP = 2 \times 10^{-5}$ and $R = 1.3 \times 10^{-3}$ (Fig. S20). To estimate the intra-chain coupling between Fe(II) ions in **4**, the 1D Fisher chain model was used[15]. The best fitting in the whole temperature range produced g = 2.25, J = −2.76 cm^{-1}, $TIP = 4\times10^{-5}$ and $R = 4.7\times10^{-3}$ (Fig. 8).

The exchange couplings of **2–6** are compiled in Table S12. They show various coupling constants ranging from 0.31 to –2.76 cm^{-1} for different bridging modes. According to the Goodenough´s rules, the μ_2-O bridge can mediate ferro- or antiferromagnetic interaction, depending on the Fe–O–Fe bond angles[16]. In **2**, the Fe–O–Fe angle is 102.96°, which lies in the range for a ferromagnetic interaction.[9e, 17] On the other hand, the type of magnetic interaction through a bridging carboxylate ligand generally depends on its coordination mode: the *syn-syn* mode usually induces antiferromagnetic interaction whereas the *syn-anti* mode normally gives rise to weak ferromagnetic interaction[18]. Moreover, if other bridges are also present (e.g. μ_2-O), they could add or counterbalance their effects. Accordingly, the antiferromagnetic coupling between Fe(II) in **3**, and the ferromagnetic exchange in **5** and **6** can be attributed to the *syn-syn* and *syn-anti* carboxylate bridging modes, respectively. For **4** which have a mixed bridging mode, the Fe–O–Fe bond angle (118.9°) mediates antiferromagnetic interaction and the *syn-anti* carboxylate bridge mediates weak ferromagnetic coupling. Consequently, the antiferromagnetic interaction in **4** can be anticipated due to the counter-complementarity effect of one μ_2-O bridge and one *syn-anti* carboxylate bridge.

It is interesting to compare the magnetic coupling constants of **5** and **6**. Although they both display the same bridging mode, i.e. bis-(*syn-anti*), the magnetic interaction in **6** is about three times larger than that in **5**. The Fe–Fe distance of **6** (4.70 Å) is smaller than that of **5** (4.81 Å). Besides, the *syn-anti* bridge in **5** adopts a equatorial-axial configuration, while that in **6** links the adjacent Fe(II) with a equatorial-equatorial fashion (Fig. S21). It has been well established that a small M–M distance can lead to a large magnetic interaction, and the *syn-anti* equatorial-axial model usually results in a small interaction. Considering the above two facts, a larger magnetic interaction in **6** than that in **5** can be easily understood.

Conclusion

In summary, six new Fe(II)-based MOFs were successfully constructed by an alternative strategy using $[Fe(Cp)(CO)_2]_2$ as a starting material under hydro-thermal condition. In addition, their structures, thermal stabilities and magnetism have been investigated. Compound **1** displays a 3D framework while **2–6** exhibit 2D layer structures that are further extended into 3D supramolecular networks through hydrogen bonding. The variable-temperature magnetic susceptibility measurements indicate that **2**, **5** and **6** exhibit ferromagnetic interactions between Fe(II) ions, whereas **3** and **4** show antiferromagnetic interactions between Fe(II) centres. Furthermore, the strategy employed in this work may provide a useful approach to the design and synthesis of novel Fe(II)-based MOFs.

Acknowledgements

This work was supported by the National Basic Research Program of China (973 Program, 2012CB821702), the National Natural Science Foundation of China (21233009 and 21173221) and the State Key Laboratory of Structural Chemistry, Fujian Institute of Research on the Structure of Matter, Chinese Academy of Sciences.

Notes and references

[a] *State Key Laboratory of Structural Chemistry, Fujian Institute of Research on the Structure of Matter, Chinese Academy of Sciences, Fuzhou, Fujian 350002, P. R. China. E-mail: swdu@fjirsm.ac.cn; Fax: (+86) 591 83709470*

[b] *University of Chinese Academy of Sciences, Beijing 100039, P. R. China.*

†Electronic Supplementary Information (ESI) available: X-ray crystallographic data, additional figures, IR, TGA and XRD pattern. For ESI and crystallographic data in CIF or other electronnic format see DOI:10.1039/b000000x/.

1 (a) B. Li, H. M. Wen, H. L. Wang, H. Wu, M. Tyagi, T. Yildirim, W. Zhou and B. L. Chen, *J. Am. Chem. Soc.*, 2014, **136**, 6207; (b) X. Zhao, X. H. Bu, T. Wu, S. T. Zheng, L. Wang and P. Y. Feng, *Nat Commun.*, 2013, **4**, 2344; (c) J. Park, L. B. Sun, Y. P. Chen, Z. Perry and H. C. Zhou, *Angew. Chem. Int. Ed.*, 2014, **53**, 5842; (d) Z. R. Herm, B. M. Wiers, J. A. Mason, J. M. Baten, M. R. Hudson, P. Zajdel, C. M. Brown, N. Masciocchi, R. Krishna and J. R. Long, *Science.*, 2013, **340**, 960; (e) R. Maurice, P. Verma, J. M. Zadrozny, S. Luo, J. Borycz, J. R. Long, D. G.Truhlar and L. Gagliardi, *Inorg. Chem.*, 2013**, 52**, 9379.

2 (a) H. Furukawa, K. E. Cordova, M. O. Keeffe and O. M. Yaghi, *Science*, 2013, **341**, 6149; (b) H. Deng, S. Grunder, K. D. Cordova, C. Valente, H. Furukawa, M. Hmadeh, F. Gandara, A. C. Whalley, Z. Liu, S. Asahina, H. Kazumori, M. O'Keeffe, O. Terasaki, J. F. Stoddart and O. M. Yaghi, *Science*, 2012, **336,** 1018; (c) Y. B. Xie, H. Yang, Z. Y. Wang, Y. Y. Liu, H. C. Zhou and J. R. Li, *Chem.*

Commun., 2014, **50**, 563; (d) J. J. Qian, F. L. Jiang, K. Z. Su, Q. P. Li, K. Zhou, M. Y. Wu, D. Q. Yuan and M. C. Hong, *CrystEngComm*., 2014, **16**, 7434.

3 (a) M. Kurmoo, *Chem. Soc. Rev*., 2009, **38**, 1353; (b) D. F. Weng**,** Z. M. Wang and S. Gao*, Chem. Soc. Rev*., 2011, **40**, 3157.

4 (a) H. L. Sun, Z. M. Wang and S. Gao, *Coord. Chem. Rev*., 2010, **254**, 1081; (b) J. J. Hou, R. Zhang, Y. L. Qin and X. M. Zhang, *Cryst. Growth Des*., 2013, **13**, 1618; (c) Q. P. Li, J. J. Qian, C. B. Tian, P. Lin, Z. Z. He, N. Wang, J. N. Shen, H. B. Zhang, T. Chu, Y. Yang, L. P. Xue and S. W. Du, *Dalton Trans.*, 2014, **43**, 3238; (d) Y. Peng, C. B. Tian, Y. H. Lan, N. Magnani, Q. P. Li, H. B. Zhang, A. K. Powell and S. W. Du, *Eur. J. Inorg. Chem*., 2013, **32**, 5534; (e) N. Wang, J. G. Ma, W. Shi and P. Cheng, *CrystEngComm*., 2012, **14**, 5634.

5 (a) J. Tao, R. J. Wei, R. B. Huang and L. S. Zheng, *Chem. Soc. Rev*., 2012, **41**, 703; (b) G. Fe′rey, F. Millange, M. Morcrette, C. Serre, M. L. Doublet, J. M. Greneche and J. M. Tarascon, *Angew. Chem. Int. Ed*., 2007, **46**, 3259; (c) E. D. Bloch, W. L. Queen, R. Krishna, J. M. Zadrozny, C. M. Brown and J. R. Long, *Science*, 2012, **335**, 1606; (d) S. Goswami, A. Adhikary, H. Sekhar Jena, S. Biswas and S. Konar, *Inorg. Chem.*, 2013, **52**, 12064.

6 (a) Serre. C, Millange. F, Thouvenot. C, N. M. Marsolier, G. Louer, and G. Fe´rey, *J. Am. Chem. Soc*., 2002, **124**, 13519. (b) M. Sanselme, J. M. Grenèche, M. R. Cavellec and G. Férey, *Chem. Commun*., **2002**, 2172; (c) Barthelet. K, Marrot. J, G. Fe´rey and D. Riou, *Chem. Commun*., 2004, 520.

7 A. C. Sudik and O. M. Yaghi, *Inorg. Chem*., 2005, **44**, 2998.

8 (a) S. J. Liu, L. Xue, T. L. Hu and X. H. Bu, *Dalton Trans.,* 2012, **41**, 6813; (b) Y. Q. Wei, Y. F. Yu, R. J. Sa, Q. H. Li and K. C. Wu, *CrystEngComm*., 2009, **11**, 1054; (c) W. Wang, J. Y. Sun, D. J. Zhang, T. Y. Song, W. Song, L. Y. Zhang, Y. Li Chen, Y. Fan and P. Zhang, *Inorg. Chim. Acta*, 2012, **384**, 105; (d) Z. B. Han, J. Li and J. Q. Gao, *J. Coord. Chem*., 2006, **59**, 1641; (e) S. H. Yan, X. J. Zheng, L. C. Li, D. Q. Yuan and L. P. Jin, *Dalton Trans*., 2011, **40**, 1758.

9 (a) S. R. Miller, D. Heurtaux, T. Baati, P. H. Jada, J. M. Greneche and C. Serre, *Chem. Commun*., 2010, **46**, 4526; (b) Y. Liang, W. Li and B. J. Guo, *Acta Cryst.*, 2005, **E61**, 1782; (c) S. W. Ng, *Acta Cryst*., 2008. **E64**, 728; (d) L. J. Hao and T. L. Yu, *Acta Cryst.*, 2007, **E63**, 1926; (e) C. B. Tian, H. B. Zhang, Y. Peng, Y. E. Xie, P. Lin, Z. H. Li and S. W. Du, *Eur. J. Inorg. Chem.,* 2012, **25**, 4029.

10 *CrystalClear, version 1.36,* Molecular Structure Corp. and Rigaku Corp., The Woodlands, TX, and Tokyo, Japan, 2000.

11 G. M. Sheldrick, SHELXS 97, *Program for Crystal Structure Solution,* University of Göttingen, Göttingen, Germany.

12 (a) C. P. Li and M. Du, *Chem. Commun*., 2011, **47**, 5958; (b) V. R. Pedireddi and S. Varughese, *Inorg. Chem*., 2004, **43**, 450; (c) L. L. Qu, Y. L. Zhu, Y. Z. Li, H. B. Du and X. Z. You, *Cryst. Growth Des.*, 2011, **11**, 2444; (d) G. H. Xu, X. Y. He, J. Y. Lv, Z. G. Zhou, Z. Y. Du and Y. R. Xie, *Cryst. Growth Des.*, 2012, **12**, 3619; (e) L. Luo, K. Chen, Q. Liu, Y. Lu, G. C. Lv, Y. Zhao and W. Y. Sun, *Cryst. Growth Des*., 2013, **13**, 2312.

13 (a) E. V. Alexandrov, V. A. Blatov, A. V. Kochetkov and D. M. Proserpio, *CrystEngComm*., 2011, **13**, 3947; (b) V.A. Blatov, *IUCr Compcomm Newsl*., 2006, **7**, 4.

14 (a) T. Liu, Y. J. Zhang, Z. M. Wang and S. Gao, *Inorg. Chem.,* 2006, **45**, 2782; (b) W. T. Liu, J. Y. Li, Z. P. Ni, X. Bao, Y. C. Ou, J. D. Leng, J. L. Liu and M. L. Tong, *Cryst. Growth Des*., 2012, **12**, 1482.

15 M. E. Fisher, *Am. J. Phys.,* 1964, **32**, 343.

16 J. B. Goodenough, Magnetism and the Chemical Bond, *Wiley*, New York, 1963

17 (a) J. M. C. Juan, C. Mackiewicz, M. Verelst, F. Dahan, A. Bousseksou, Y. Sanakis and J. P. Tuchagues, *Inorg. Chem.*, 2002, **41**, 1478; (b) Y. W. Li, J. P. Zhao, L. F. Wang and X. H. Bu, *CrystEngComm*., 2011, **13**, 6002.

18 S. Durot, C. Policar, G. Pelosi, F. Bisceglie, T. Mallah and J. P. Mahy, *Inorg Chem.*, 2003, **42**, 8072.

